Alpha-particle breakup at incident energies of 20 and 40 MeV/nucleon

J. R. Wu,* C. C. Chang, H. D. Holmgren, and R. W. Koontz
Department of Physics and Astronomy, University of Maryland, College Park, Maryland 20742
(Received 19 April 1979)

The breakup of alpha particles at incident energies of 20 and 40 MeV/nucleon on ^{27}Al, ^{58}Ni, ^{90}Zr, and ^{209}Bi has been studied. It was found that the breakup cross section decreases rapidly with increasing angles and increases with increasing target mass and incident energy. The total breakup yield, summed over all charged fragments, is ~15–35% of the alpha-particle total reaction cross section, and has an approximate $A^{1/3}$ dependence. The ratios of breakup yields among different fragments are approximately $p:d:t:{}^3\mathrm{He} \approx 13:3:1:2$, and are roughly independent of the incident energy and the target nucleus. These features suggest that the alpha-particle fragmentation is a peripheral process and is dominated by the properties of the incident projectile. A simple plane-wave alpha-particle breakup model gives a rather good description to the experimental data. In addition to the breakup deuteron peak at half of the beam energy, a second peak at quarter of the beam energy (or the same energy as the breakup proton peak) is observed. This peak might be due to a two-step breakup-pickup process.

[NUCLEAR REACTIONS ^{27}Al, ^{58}Ni, ^{90}Zr, ^{209}Bi(α, xp), (α, xd), (α, xt), $(\alpha, x{}^3\mathrm{He})$, $E_\alpha = 80$, 160 MeV; $\theta = 6°$–$30°$, measured $d^2\sigma/d\Omega dE$, deduced alpha-particle breakup yield, Comparisons with alpha-particle breakup model.]

I. INTRODUCTION

In a previous paper[1] we reported evidence for the alpha-particle breakup process at an incident energy of 35 MeV/nucleon. The breakup process was suggested by broad peaks in the 20° to 30° spectra of protons, deuterons, tritons, and ^{3}He at an energy corresponding to the beam velocity. This suggestion was substantiated by more detailed studies of the ^{3}He spectra over the angular range from 13° to 20° for five targets spanning the periodic table. The spectral shapes and angular distributions were found to be essentially independent of the target. The total yield of the ^{3}He breakup peak for each target was roughly constant when divided by $A^{1/3}$, suggesting that the alpha particle breaks up in the nuclear periphery. The features of the spectral shapes and angular distributions were well fitted with a simple breakup model[2] using an internal alpha-particle wave function[3] consistent with the results of $^4\mathrm{He}(p, 2p)^3\mathrm{H}$ studies.[4] The observation of the alpha-particle breakup process at 43 MeV/nucleon, and distorted-wave Born approximation (DWBA) breakup analysis of those results has been recently reported.[5] Projectile breakup has also been observed in more loosely bound projectiles such as d,[6,7] ^{3}He,[8] ^{6}Li,[9] and heavy ions.[10]

As part of a systematic study of the alpha-particle breakup process, we have extended our measurements of the inclusive spectra to include all charged-particle breakup channels (p, d, t, and ^{3}He) down to 6° for four target nuclei, ^{27}Al, ^{58}Ni, ^{90}Zr, and ^{209}Bi, at incident energies of 20 and 40 MeV/nucleon. Our objective in these measurements was to investigate

(1) the dependence of the breakup yield on alpha-particle bombarding energy,
(2) the dependence of the breakup yield on target nuclei,
(3) the distribution of the breakup yield among the various channels,
(4) the angular variation and the spectral shapes of the breakup yield for each channel, and
(5) the total breakup cross section.

In addition, a series of coincidence studies of the breakup process have been carried out to help identify the possible reaction mechanisms involved in alpha-particle breakup. The results of the coincidence experiments will be presented in a later paper.[11]

II. EXPERIMENTS

In this series of experiments, alpha particles accelerated to 80 and 160 MeV by the University of Maryland Cyclotron were used to bombard ^{27}Al (1.72 mg/cm^2), ^{58}Ni (1.02 mg/cm^2), ^{90}Zr (1.06 mg/cm^2), and ^{209}Bi (0.9 mg/cm^2) targets. The primary interest was to measure the very forward angle spectra of the light charged particles ($Z \leq 2$, $A \leq 4$) over an energy range extending from somewhat above the evaporation peak to the maximum kinematically allowed energy. Two triple-counter telescopes were employed to detect all the light charged particles so as to span the complete energy spectrum for each particle. The

detector solid angles were typically of the order of 0.1 msr.

The details of the experimental methods, including electronics, data collection, reduction, and error analyses are described in Ref. 6. The overall uncertainties for the experimental data are generally less than 10%.

It was extremely important to achieve a highly monochromatic beam, as the projectile breakup yield is concentrated at forward angles where beam impurity effects would be most pronounced. The experiments were carried out in one of the high-resolution, low-background upper experimental areas. The beam was first momentum analyzed by a 90° analyzing magnet. Two sets of "clean up" slits at intermediate foci following a second 90° analyzing magnet and the 20° bend of the switching magnet were used to minimize beam halo. Measurements at 6° with a blank target frame indicated there was essentially no background. The cyclotron ion source was also turned down so as to produce a beam of ~1000 particles per second (beam optics held constant) and a detector was placed in the direct beam. The observed spectrum was consistent with a monoenergetic beam incident on the detector. A low energy tail present in the observed spectrum could be entirely accounted for by calculations of the reactions tails in the detector (which were corrected for in the data analysis). The beam energy resolution was typically 20/40 keV (80/160 MeV) and the overall energy resolution of the order of 100 keV for ^{3}He particles and 400 keV for $Z = 1$ particles. The final energy spectra, however, were summed into 1 MeV energy bins to reduce the statistical fluctuations of the broad peaks.

III. RESULTS

Differential energy spectra of p, d, t, ^{3}He, and alpha particles were measured for ^{27}Al, ^{58}Ni, ^{90}Zr, and ^{209}Bi over the angular range from 6° to 30°. Table I summarizes the experimental conditions and some of the results.

Figures 1(a)–1(g) exhibit the energy spectra for p, d, t, and ^{3}He resulting from 80 and 160 MeV alpha particles. The general features of these spectra can be summarized as follows:

(1) Broad bumps are seen in each spectrum for all targets at both energies for angles less than 30°.

(2) These broad peaks are centered at an energy corresponding approximately to the beam velocity, i.e., peaked at $E_x \simeq (m_x/m_\alpha)E_\alpha$ (see Table I) for all particles and targets, where E_x, E_α, m_x, and m_α are the laboratory energies and masses of the observed particle x and incident alpha particle. The peak locations shift slightly toward lower energies with increasing angle.

(3) The breakup yields vary rapidly with the angle and are concentrated within a forward cone of width $\Delta\theta_x$, consistent with the estimation

$$\Delta\theta_x \simeq \frac{p_x m_\alpha}{p_\alpha m_x} = \left(\frac{m_\alpha \epsilon_x}{m_x E_\alpha}\right)^{1/2},$$

where p_x is the average internal momentum of x, p_α, the laboratory momentum of the incident alpha particle, and ϵ_x the separation energy of x from α.

(4) The shapes of the breakup spectra do not depend significantly on the target nucleus.

(5) The widths of breakup peaks increase with increasing bombarding energy (see Table I).

(6) The breakup yields show an $A^{1/3}$ target dependence. This feature can be seen in Fig. 2, where the comparison of particle energy spectra divided by $A^{1/3}$ is shown for four nuclei.

(7) The cross sections of breakup peaks are larger for p and ^{3}He than for d and t, and the peak width is wider for p and d than for t and ^{3}He. The total breakup yields decrease in the order of p, d, ^{3}He, and t (see Table I).

These general features of the broad bumps seen in all forward angle spectra of p, d, t, and ^{3}He are clearly consistent with peripheral fragmentation of the projectile in which the behavior of the peak is determined by the properties of the incident projectile.

The breakup peaks for all particles lie on an underlying continuum due to pre-equilibrium emission which extends to large angles. From our previous studies[1,12] we know that the pre-equilibrium yields also increase rapidly with decreasing angle but tend to have a somewhat flat energy distribution at forward angles for particles with mass near the projectile mass (^{3}He and t). This continuum is somewhat difficult to estimate, as existing theories do not reliably predict the angular dependence of pre-equilibrium yields. In the case of the breakup proton peaks, the tails of the proton evaporation yield cause an additional background problem. This problem is more serious at 20 MeV/nucleon, where not only is the relative contribution of the breakup to evaporation yield smaller but the separation between the peaks is less than it was at 40 MeV/nucleon. In the case of the t and ^{3}He spectra, a different problem arises in that the high energy tails of the breakup peaks extend into the region of discrete peaks, which come from the formation of a high angular momentum state via stripping reactions.[13] Again, both the relative intensities of the breakup peak and discrete states and the separation of these

TABLE I. Summary of experimental conditions and results and some of the calculated results.

Target and incident energy	Angles observed (degree)	Particle observed	Low energy cutoff (MeV)	Breakup peak location at 6° (MeV)	Breakup peak width at 6° (MeV)	Breakup peak cross section at 6° (mb/sr/MeV)	Calculated breakup peak location at 6° (MeV)	Calculated breakup peak width at 6° (MeV)
^{27}Al $E=80$ MeV	6,8,10, 12,14,16, 18,20,22, 26,32,36, 40	p	8.45	22	36	7.1	24	35
		d	9.45	45	30	3.7	43	31
		t	10.45	...[a]	...[a]	...[a]	...[a]	...[a]
		^{3}He	7.45	...[a]	...[a]	...[a]	...[a]	...[a]
^{58}Ni $E=80$ MeV	6,8,10, 12,14,16, 18,20,22, 26	p	8.45	23	36	10.6	24	35
		d	9.45	45	30	5.0	41	32
		t	10.45	...[a]	...[a]	...[a]	53	18
		^{3}He	7.45	...[a]	...[a]	...[a]	...[a]	...[a]
^{90}Zr $E=80$ MeV	6,8,10, 12,14,16, 18,20,22, 24,26,28, 30	p	8.45	24	32	11	24	34
		d	9.45	45	30	5.2	40	32
		t	10.45	...[a]	...[a]	...[a]	52	20
		^{3}He	7.45	...[a]	...[a]	...[a]	...[a]	...[a]
^{27}Al $E=160$ MeV	6,8,10, 14,18,22, 26,30	p	17.19	42	52	12.8	44	50
		d	18.99	85	56	4.8	82	58
		t	22.59	123	46	5.3	121	43
		^{3}He	51.39	127	44	9.3	124	43
^{58}Ni $E=160$ MeV	6,8,10, 14,18,22, 26,30	p	17.19	41	52	17.2	44	50
		d	18.99	84	56	5.9	82	56
		t	22.59	122	44	6.3	120	40
		^{3}He	51.39	128	44	10.0	123	41
^{90}Zr $E=160$ MeV	6,8,10, 14,18,20, 26,30	p	17.19	42	52	19.5	44	49
		d	18.99	84	56	7.2	82	56
		t	22.59	121	44	8.7	119	39
		^{3}He	51.39	129	40	19.6	123	41
^{209}Bi $E=160$ MeV	6,8,10, 14,20,26, 30	p	17.19	42	50	23.6	44	48
		d	18.99	84	52	9.5	81	54
		t	22.59	115	42	12.6	114	35
		^{3}He	51.39	125	40	28.8	123	41

[a] It is difficult to estimate due to a number of sharp peaks.

regions are more serious at 20 MeV/nucleon than at 40 MeV/nucleon.

In order to extract total and differential cross sections in a consistent manner, we have fitted an extension of the simple plane-wave projectile breakup calculations, which were used in Ref. 1 and are discussed in the next section, to the data at the lowest angle (6°). In the case of ^{3}He and t, where the pre-equilibrium yields are relatively flat, we have emphasized the fit to the lower energy part of the breakup peak in order to minimize the contribution from the discrete states. In the case of p and d, we have emphasized the fit to the high energy part of the breakup peak where the pre-equilibrium and evaporation yields are expected to be less important.

A second peak appears in the deuteron spectra at approximately $\frac{1}{4}E_\alpha$ (i.e., at the same energy as the breakup proton peak). This peak is particularly pronounced compared to the breakup deuteron peak at 40 MeV/nucleon for light target nuclei. Additional measurements have established

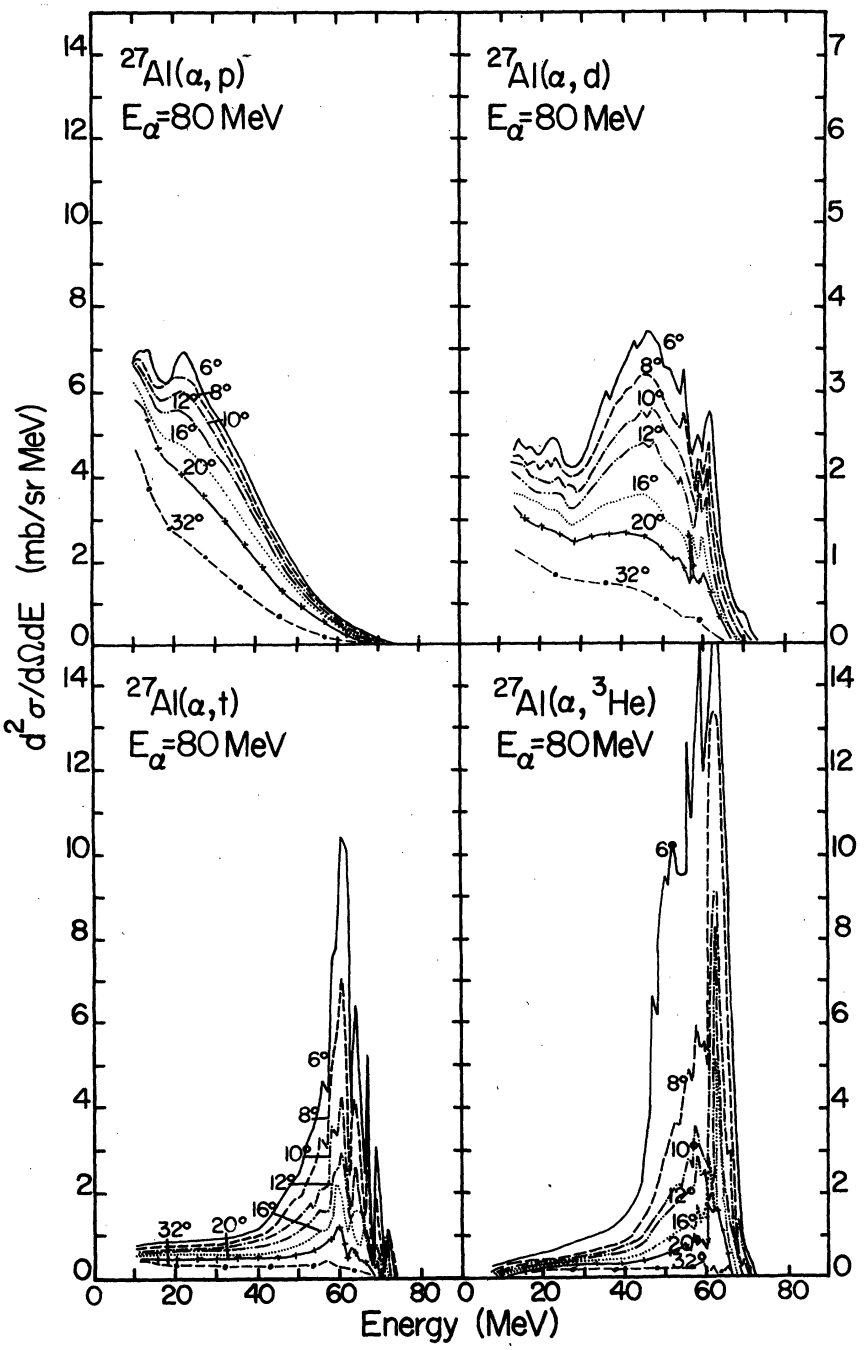

FIG. 1. (a) The differential energy spectra of p, d, t, and ^{3}He resulting from the bombardment of 80 MeV alpha particles on ^{27}Al. The arrows indicate the location of beam velocity. (b) Same as (a) for 80 MeV alpha on ^{58}Ni. (c) Same as (a) for 80 MeV alpha on ^{90}Zr. (d) Same as (a) for 160 MeV alpha on ^{27}Al. (e) Same as (a) for 160 MeV alpha on ^{58}Ni. (f) Same as (a) for 160 MeV alpha on ^{90}Zr. (g) Same as (a) for 160 MeV alpha on ^{209}Bi.

that this peak is not the result of particle identification problems, slit edge scattering, beam contaminants, or halos. Furthermore, the yield of this peak decreases less rapidly with angle than the breakup deuteron peak (at $\frac{1}{2}E_\alpha$), and its yield relative to the breakup deuteron peak decreases with increasing target mass and decreasing incident energy. It is interesting to note that this peak occurs at the same energy as the breakup proton peak and that the proton peak also

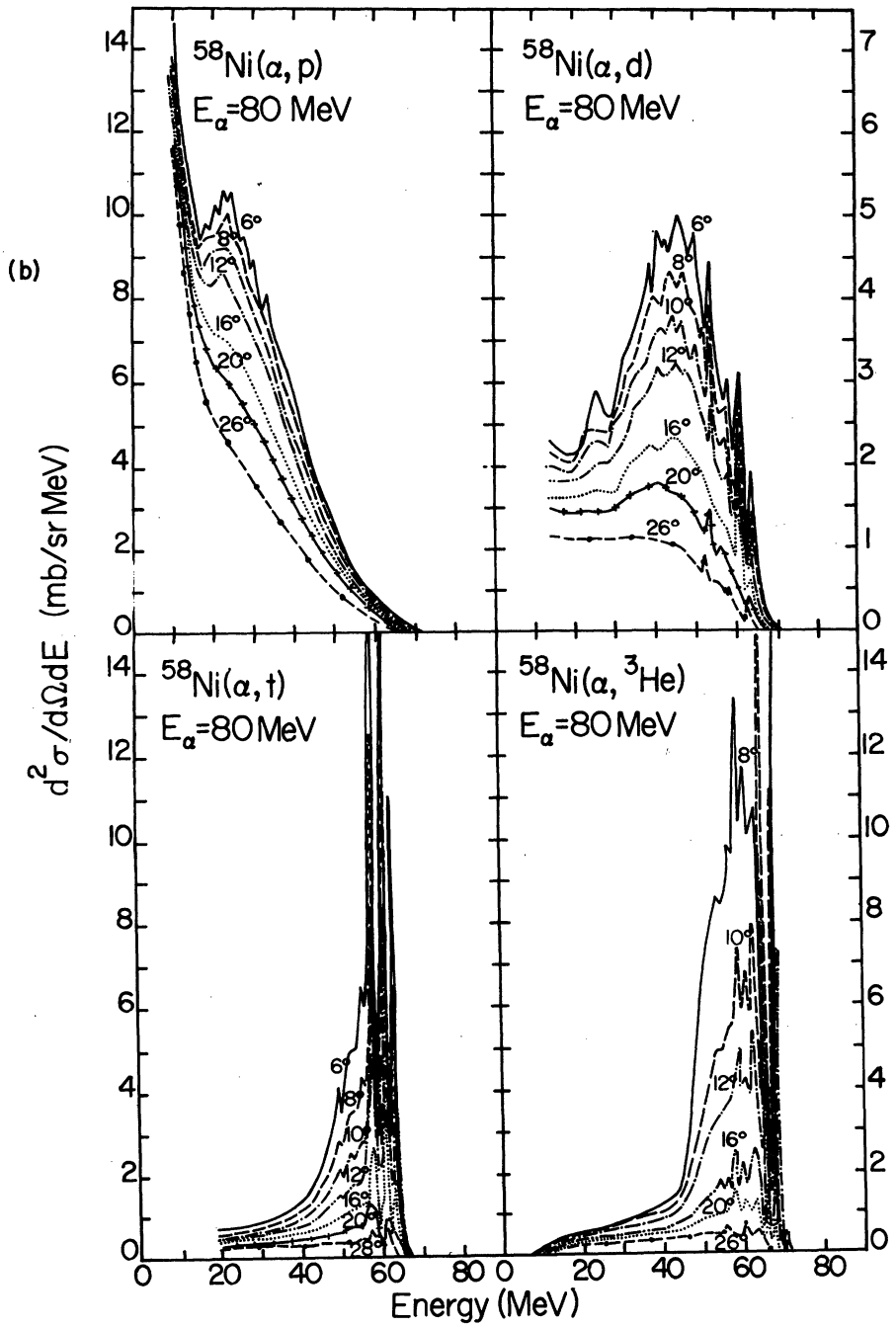

FIG. 1. (*Continued*).

decreases less rapidly with angle than the breakup deuteron peak. A possible explanation of this second deuteron peak is suggested in the next section.

IV. DISCUSSION

Several mechanisms have been suggested to account for projectile breakup.[1,5-10] The initial

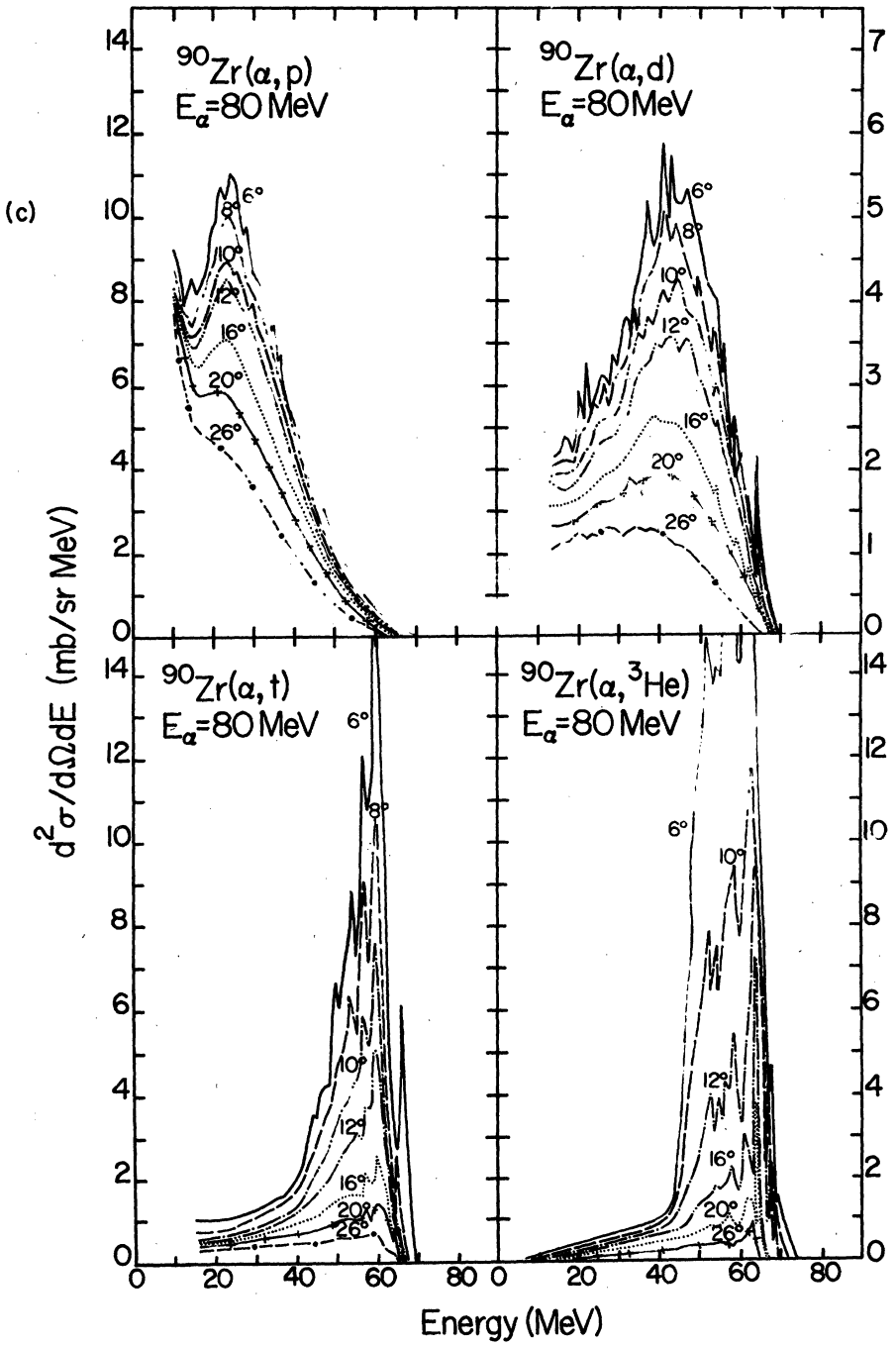

FIG. 1. (*Continued*).

results from our coincidence studies of the breakup process[11] indicate that at least three different mechanisms contribute to alpha-particle breakup, but that the yield is dominated by events in which the breakup fragment is observed in coincidence with low energy evaporation particles. This result is consistent with the plane-wave breakup model of Ref. 1 if the unobserved component of the projectile is absorbed, forming a compound system with the target nucleus. Such a process cor-

(d)

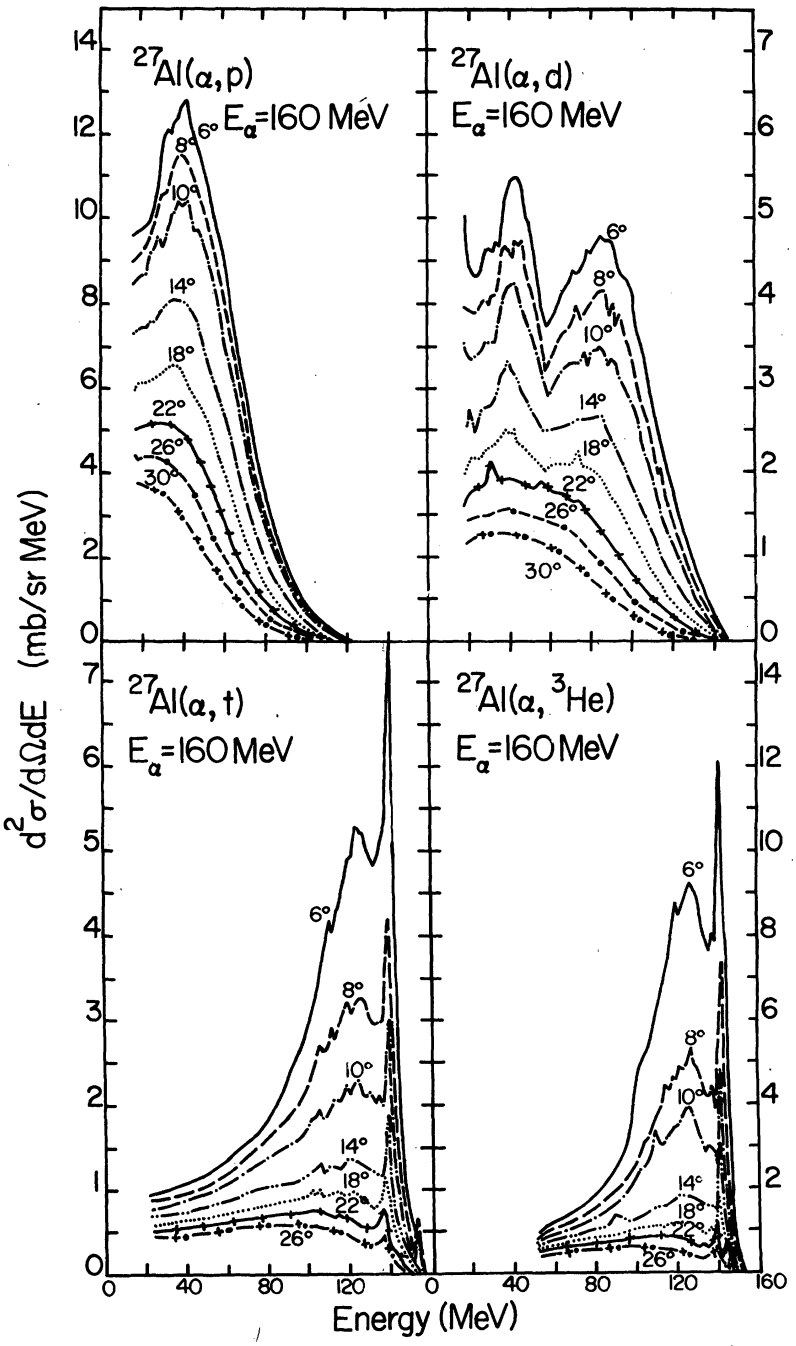

FIG. 1. (*Continued*).

responds to stripping to a highly excited continuum of the compound system, where the density of states is sufficiently high such that the energy and angular behavior of the spectra are determined primarily by the internal momentum distribution and kinetic energy of the incident projectile.

Although a DWBA analysis will be required to understand more completely the absolute magnitude of the breakup cross section, a number of physical insights are provided by the simple plane-wave breakup model of Ref. 1. Most of the features of the energy and angular distributions are reasonably well described by this model when

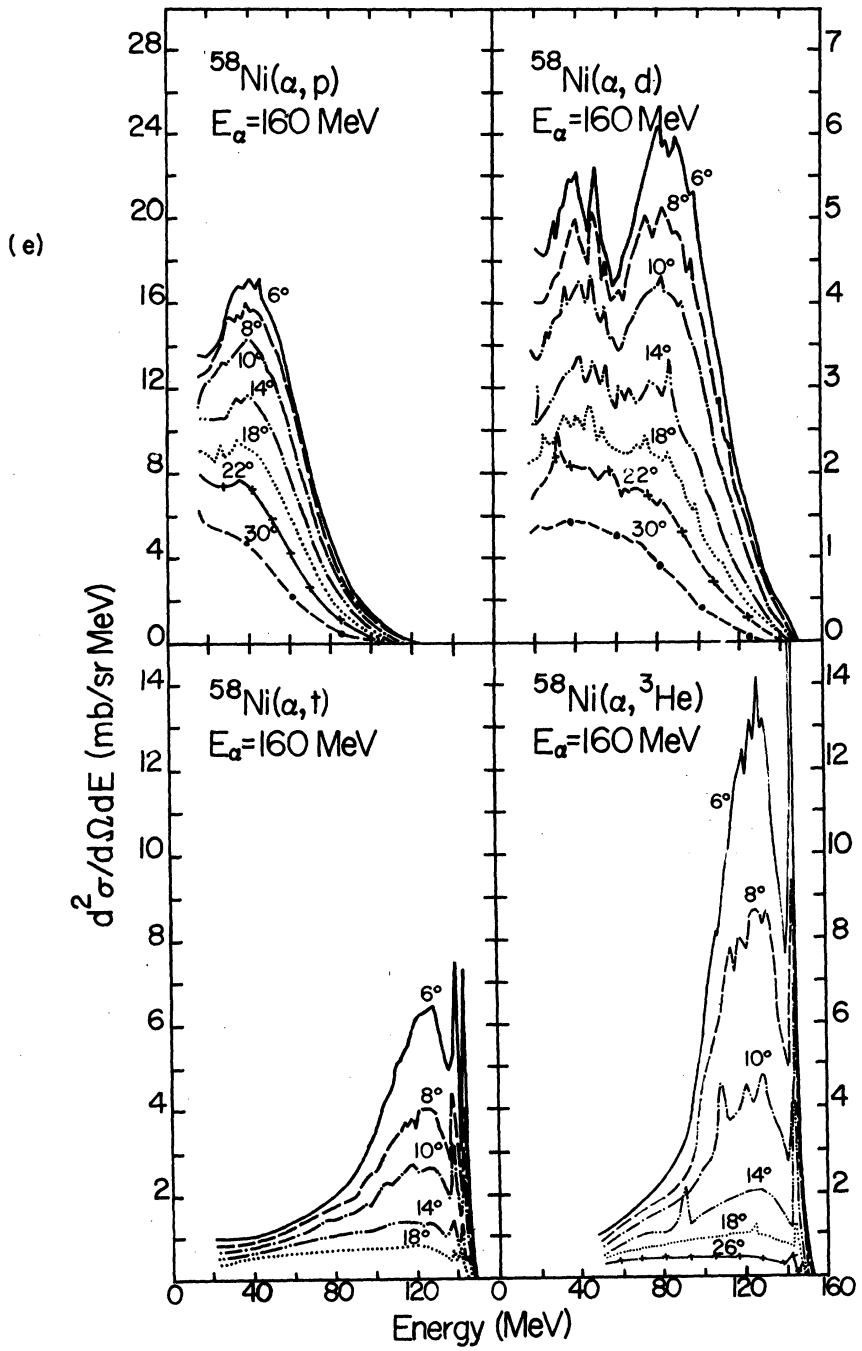

FIG. 1. (*Continued*).

an internal alpha-particle wave function is used, which gives a good fit to the ^{4}He$(p, 2p)$ results[4] and electron scattering data on ^{4}He. The model assumes absorption of constituents by the target, which gives the $A^{1/3}$ target dependence characteristic of peripheral processes. We have used this model primarily to obtain a consistent procedure for extracting the total breakup cross section from our data. In the future we hope to carry out more extensive DWBA analyses of our results, but even such calculations will be subject to the problem of how to include interference effects between the breakup process and the underlying pre-equilibrium continuum and high lying discrete

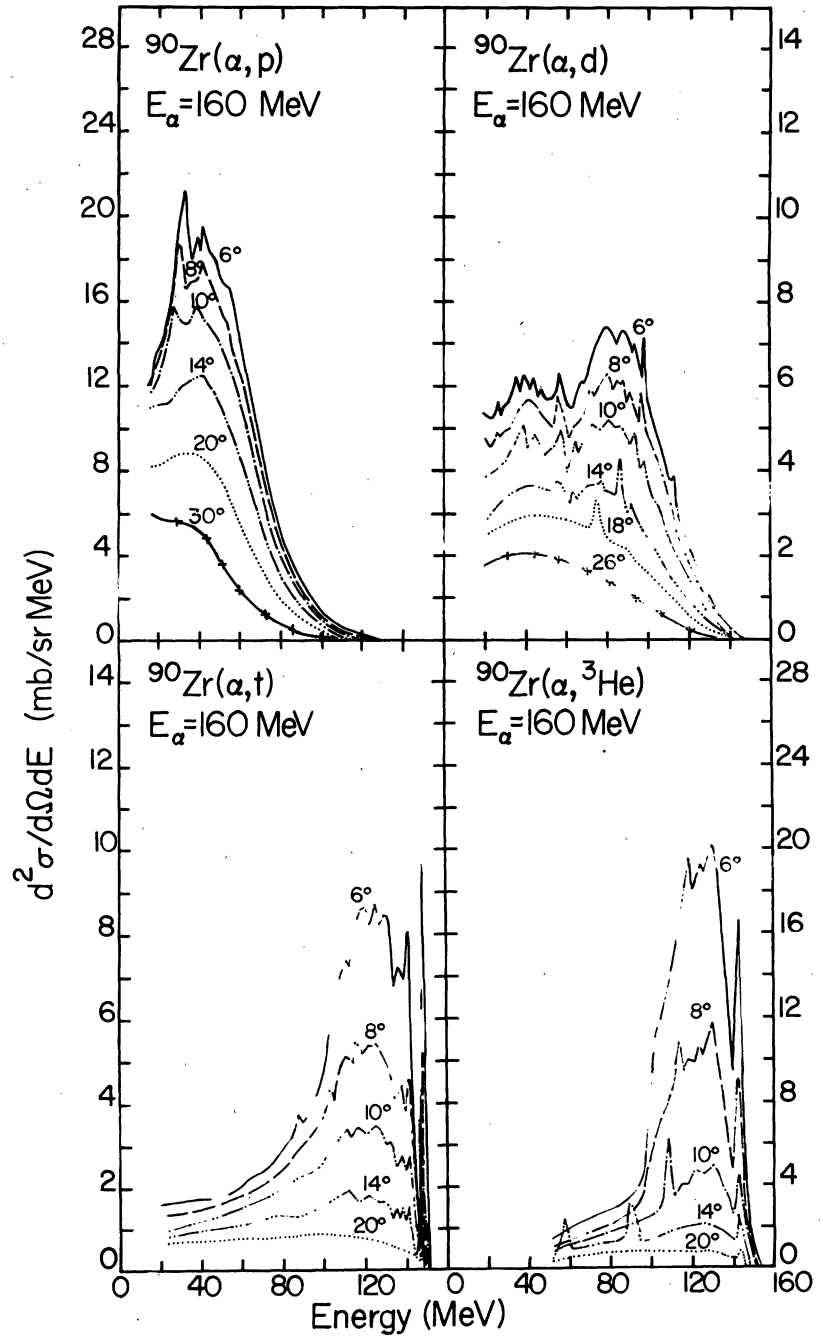

FIG. 1. (*Continued*).

states.

We have here extended somewhat the plane-wave breakup calculation which was used in Ref. 1. The cross section for the observed particle can be written in the form

$$\frac{d^2\sigma}{d\Omega_x dE_x} = N_x m_x (2m_x E_x)^{1/2} |\phi(\vec{p})|^2 \sigma_{yA}(E_y) , \qquad (1)$$

where N_x, m_x, and E_x are the normalization constant, the mass, and the kinetic energy of the ob-

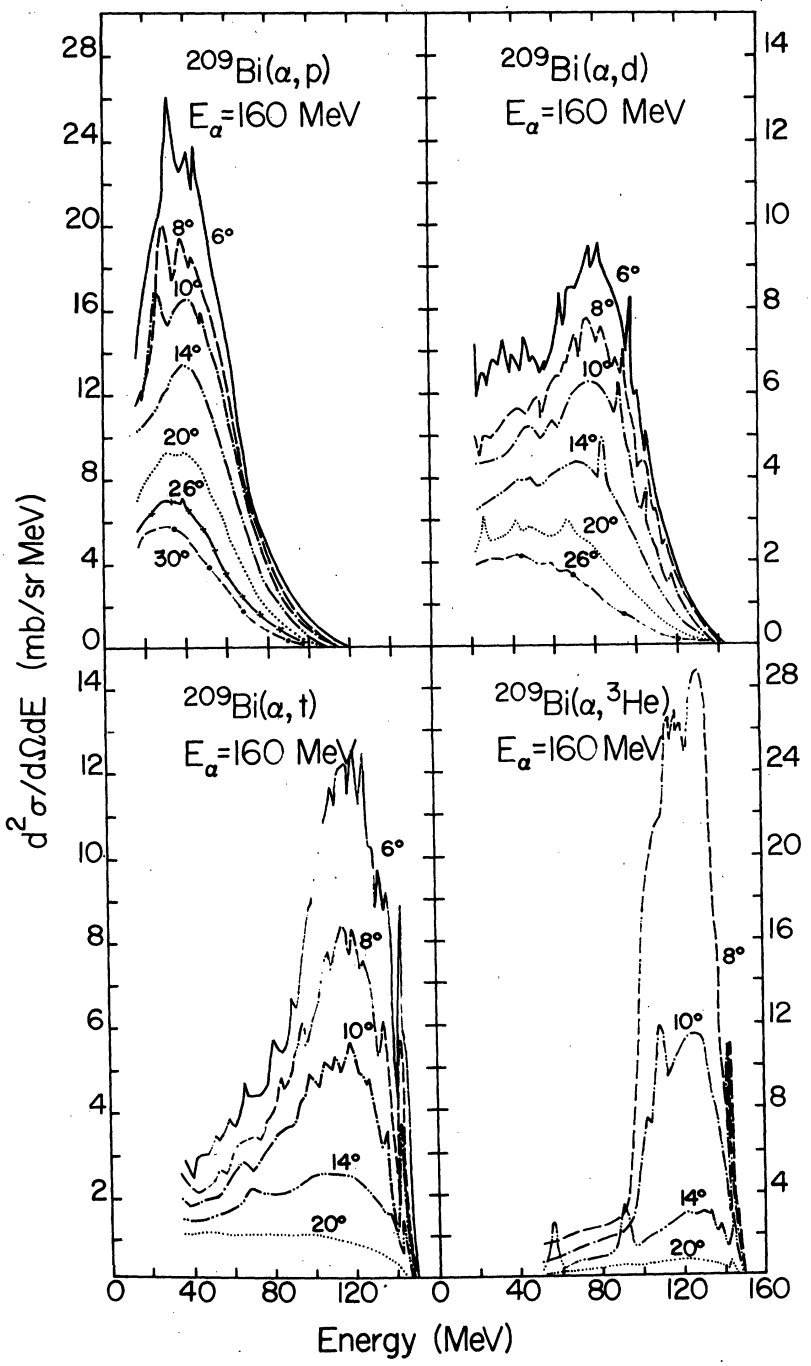

FIG. 1. (*Continued*).

served particle, respectively. σ_{yA} is the reaction cross section for the constituent $y=(\alpha-x)$ on the target nucleus A at the energy $E_y=E_\alpha-E_x-\epsilon_x$. The momentum of the observed particle, $\vec{p}_x$, is the sum of the momenta due to the motion of the incident alpha particle c.m., $\vec{p}_0$ [i.e., $(m_x/m_\alpha)\vec{p}_\alpha$], and the internal momentum of particle x, $\vec{p}=\vec{p}_x-\vec{p}_0$:

$$\phi(\vec{p})=\frac{1}{h^{3/2}}\int\psi_\alpha(r)\exp\left(\frac{i}{\hbar}\vec{p}\cdot\vec{r}\right)d^3r \qquad (2)$$

is the Fourier transform of the relative wave function of the constituents (e.g., p-t, d-d and

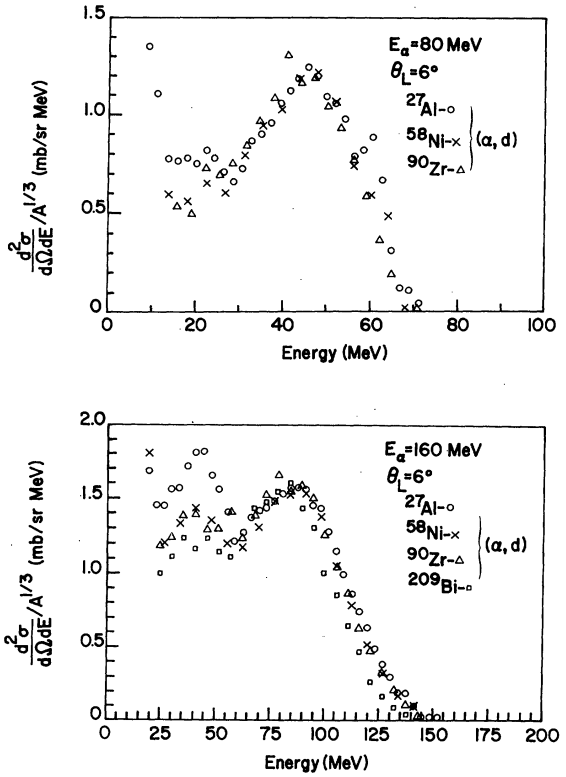

FIG. 2. Comparisons of 6° deuteron energy spectra resulting from the bombardment of 80 MeV alpha on ^{27}Al, ^{58}Ni, and ^{90}Zr and 160 MeV alpha on ^{27}Al, ^{58}Ni, ^{90}Zr, and ^{209}Bi, where the cross section has been divided by $A^{1/3}$.

^{3}He-n) in an alpha particle. A wave function of the Eckart form is used,[3]

$$\psi_\alpha(r) = C\left(\frac{\alpha}{2\pi}\right)^{1/2}\frac{e^{-\alpha r}}{r}(1-e^{-\beta r})^4, \tag{3}$$

where $\alpha = (2\mu\epsilon_x)^{1/2}/\hbar$, with μ and ϵ_x being the reduced mass and the appropriate separation energy, and C is a normalization constant. The parameter β was determined by fits from elastic electron scattering data on ^{4}He. It also fits the momentum distribution found in the quasifree scattering reactions such as ^{4}He$(p, 2p)^3$H.[4] This form of ψ_α is used for the deuteron channel with appropriate separation energy, although it has not been fitted to ^{4}He$(p, pd)^2$H data.

Figures 3 and 4 show the breakup model calculations compared with the experimental p, d, t, and ^{3}He energy spectra at several angles for 80 and 160 MeV alpha particles incident on ^{90}Zr. As indicated previously, the calculated cross sections have been normalized to the experimental peak cross section at $\theta_L = 6°$ for each observed particle at each of the two beam energies.

A similar quality of fits to the other targets was also obtained. The peak locations, peak widths, and angular dependences are rather well reproduced by the calculations. Disagreement between the calculation and experimental data is, of course, expected in regions where pre-equilibrium, evaporation, or discrete state yields are important.

The total breakup yield for each constituent was estimated by integrating the normalized expression of Eq. (1) over energy and angle. The resulting estimated breakup yields for each particle channel, target, and incident energy are summarized in Table II, where total reaction cross sections σ_R and geometrical cross sections σ_g are also given. Figure 5 shows the total breakup yield as a function of target mass. The magnitude of the breakup yield increases with the target mass approximately as $A^{1/3}$, i.e., $\sigma_{\text{breakup}} \sim 65A^{1/3}$ mb and $138A^{1/3}$ mb for $E_\alpha = 80$ and 160 MeV, respectively (see Figs. 2 and 6, and Table II). According to the plane-wave breakup model, the cross section for alpha-particle breakup is predicted to be proportional to $\frac{1}{2}\pi R R_\alpha$,[2] where R_α is the mean alpha-particle radius

$$R_\alpha = \int r|\psi_\alpha(r)|^2 d^3r$$

and $R = r_0 A^{1/3}$. The alpha-particle radius effectively determines the thickness of the peripheral width which can contribute to the yield. The different constituents may, however, suffer differing absorptions. The expression for the breakup cross section can be generalized to allow for this possibility by writing $\sigma_x = 2\pi R \Delta R_x$, where ΔR_x is the peripheral width which contributes to the reaction for the observation of constituent x. The results for ΔR_x are also listed in Table II assuming $R = 1.5A^{1/3}$ fm.

As summarized in Table II, the total breakup yield of charged particles constitutes a significant fraction of the total reaction cross section of the order of 15–35%. (If the breakup neutron yield is comparable to the proton yield, the total breakup cross section could account for as much as 50% of the total reaction cross section at 160 MeV.) The breakup yield increases with increasing bombarding energy (approximately a factor of 2 from 80 to 160 MeV), but the ratios of breakup yield among different channels ($p:d:t:{}^3\text{He} \approx 13:3:1:2$) are roughly independent of the bombarding energy and target nucleus, see Table II. The independence of the ratios of constituents with respect to E_α and A indicates that the process is dominated by the properties of the incident projectile. The large difference in the total breakup yields for protons and tritons also suggests that absorption of the constituents plays an important role.

The larger yield of protons can be understood within the model in part from the larger mean-

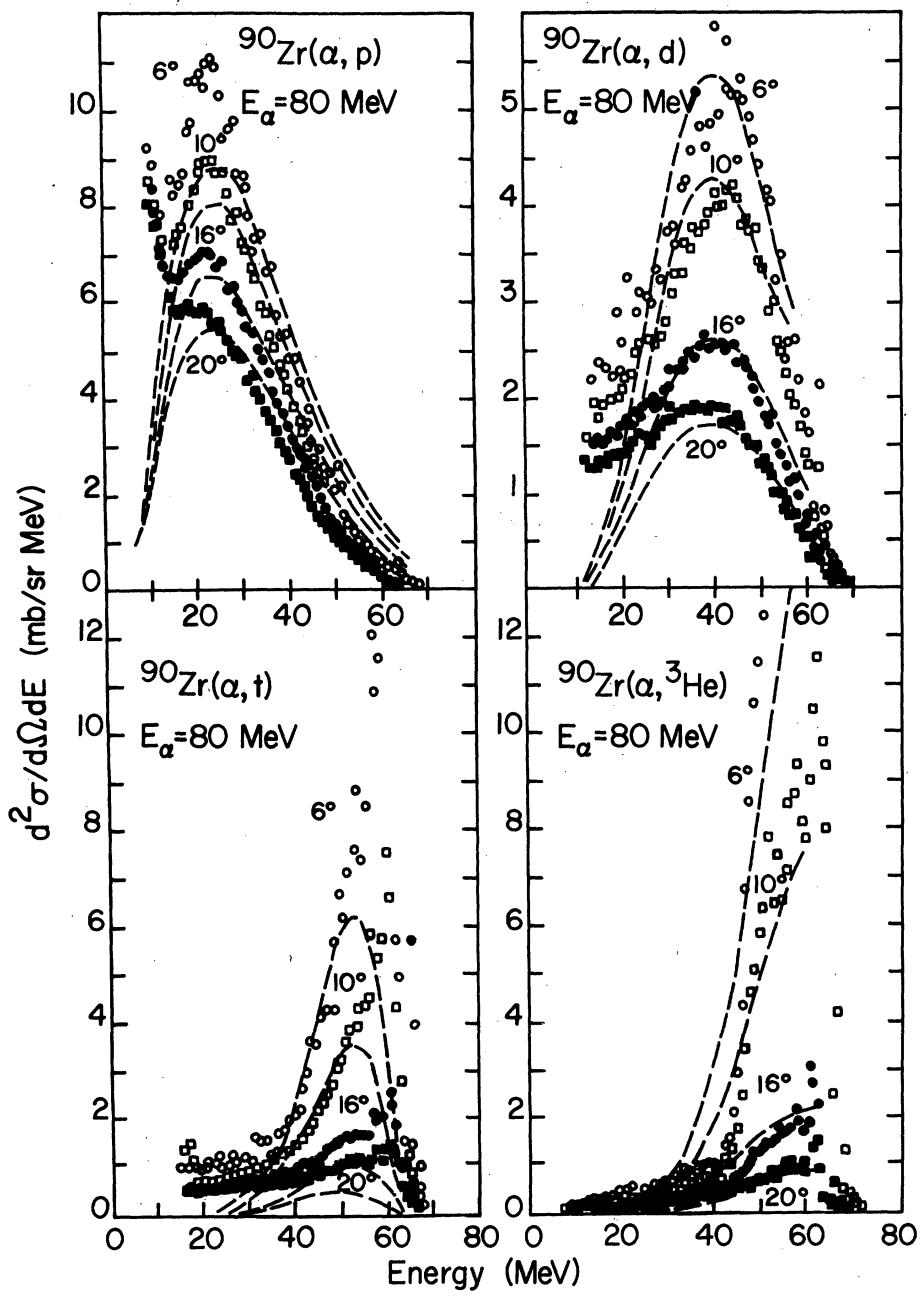

FIG. 3. Comparisons of breakup model calculations with experimental p, d, t, and ^{3}He energy spectra at several angles for 80 MeV alpha particles incident on ^{90}Zr. The calculation has been normalized to 6° spectrum for each observed particle.

free path in nuclear matter expected for protons than for the other constituents. Hence, protons can survive interactions corresponding to breakup occurring at smaller impact parameters, resulting in a larger peripheral width that can contribute to the proton yield.

The second lower energy peak in the deuteron spectra may correspond to a two-step process in which the proton (or neutron) resulting from breakup picks up a neutron (or proton). In our inclusive studies of reactions induced by 90 MeV protons[14] we found that the behavior of the continuous deuteron spectra as a function of angle and energy was very similar to that of the proton spectra, except that the yield was about a factor of 8 smaller. It was suggested that this might be

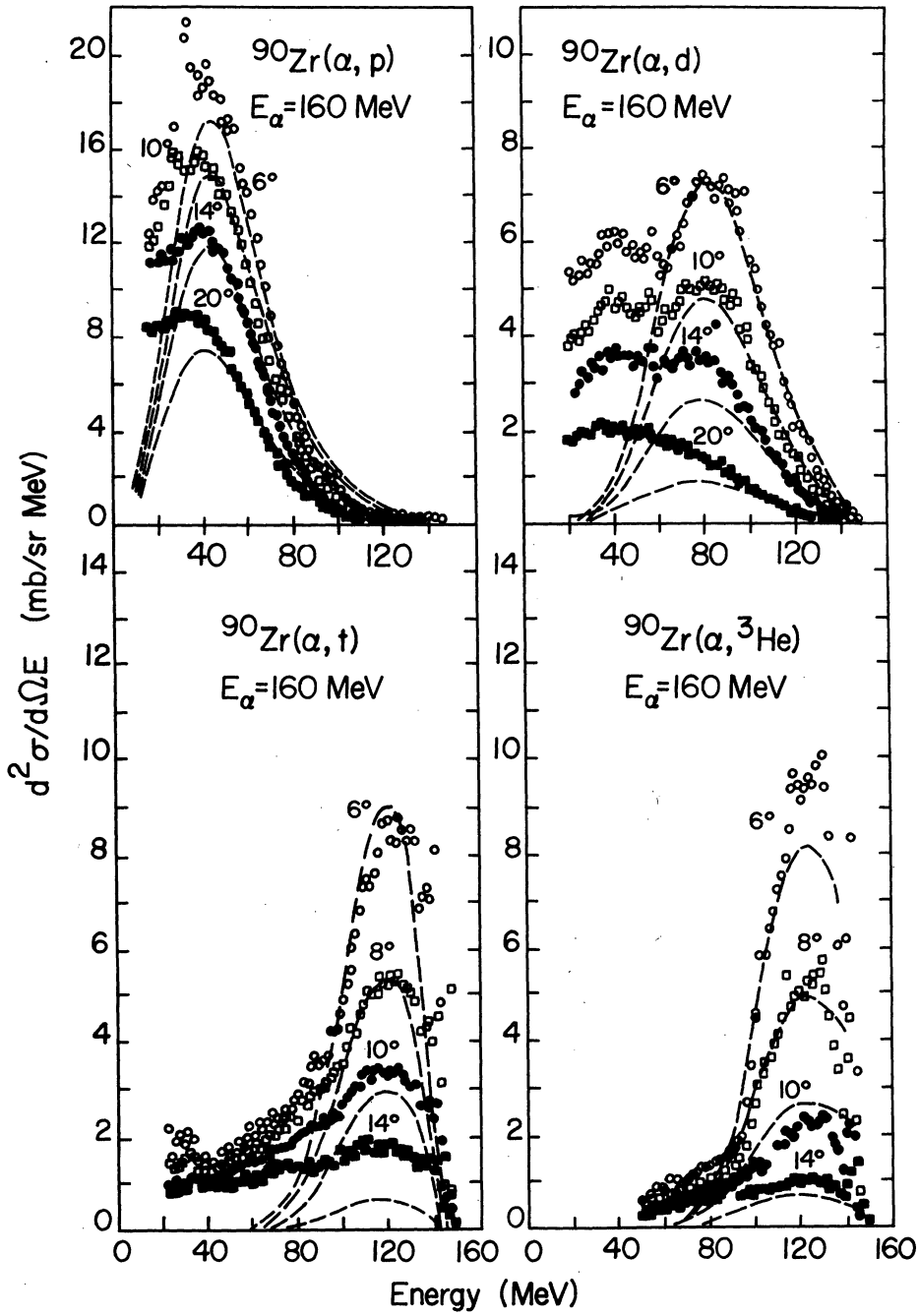

FIG. 4. Same as Fig. 3 for 160 MeV alpha particles on ^{90}Zr.

accounted for by some type of indirect pickup process. The similarity of the behavior of the second deuteron peak to the breakup proton peak, previously pointed out, suggests the possibility of a two-step process involving breakup followed by pickup. The relatively large yield of this peak for the ^{27}Al target at 40 MeV/nucleon compared to the breakup proton peak may indicate that both the proton and neutron breakup channels contribute to this process. The decreasing relative (not absolute) yield of this peak with increasing A suggests that such processes may be more favored in regions of low density nuclear matter. It should be noted that two-step processes involving the breakup of one of the initial constituents lead to peaks corresponding to the beam velocity and

TABLE II. Summary of estimated total breakup yields for each particle channel, target, and incident energy.

Target and incident energy	Total reaction cross section σ_R (mb)	Geometric cross section[a] σ_g (mb)	Particle observed	Estimated breakup cross section[b] σ_B (mb)	$\frac{\sigma_B}{\sigma_R}$	$\frac{\sigma_B}{\sigma_g}$	$\Delta R = \frac{\sigma_B}{2\pi R}$ (fm)	Estimated total breakup cross section[c] σ_t (mb)	$\frac{\sigma_t}{\sigma_R}$	$\frac{\sigma_t}{\sigma_g}$
^{27}Al			p	134 ± 15	0.108	0.090	0.474			
E = 80 MeV	1245	1488	d	31 ± 3	0.025	0.021	0.110	195 ± 16	0.157	0.131
			t	10 ± 1	0.008	0.007	0.035			
			^{3}He	20 ± 5	0.016	0.013	0.071			
^{58}Ni			p	170 ± 20	0.106	0.081	0.466			
E = 80 MeV	1610	2106	d	42 ± 6	0.026	0.020	0.115	251 ± 21	0.156	0.119
			t	13 ± 2	0.008	0.006	0.036			
			^{3}He	26 ± 4	0.016	0.012	0.071			
^{90}Zr			p	197 ± 20	0.105	0.076	0.466			
E = 80 MeV	1870	2603	d	49 ± 5	0.026	0.019	0.116	297 ± 21	0.159	0.114
			t	17 ± 2	0.009	0.007	0.040			
			^{3}He	34 ± 4	0.018	0.013	0.081			
^{27}Al			p	285 ± 25	0.248	0.192	1.008			
E = 160 MeV	1150	1488	d	56 ± 6	0.049	0.038	0.198	403 ± 26	0.350	0.271
			t	23 ± 2	0.020	0.015	0.081			
			^{3}He	39 ± 4	0.034	0.026	0.138			
^{58}Ni			p	375 ± 40	0.242	0.178	1.028			
E = 160 MeV	1550	2106	d	75 ± 7	0.048	0.036	0.206	535 ± 42	0.345	0.254
			t	30 ± 3	0.019	0.014	0.082			
			^{3}He	55 ± 10	0.036	0.026	0.151			
^{90}Zr			p	450 ± 50	0.243	0.173	1.065			
E = 160 MeV	1850	2603	d	87 ± 9	0.047	0.033	0.206	639 ± 52	0.345	0.246
			t	36 ± 4	0.019	0.014	0.085			
			^{3}He	66 ± 10	0.036	0.025	0.156			
^{209}Bi			p	530 ± 60	0.208	0.133	0.948			
E = 160 MeV	2550	3999	d	105 ± 10	0.041	0.026	0.188	800 ± 63	0.314	0.200
			t	49 ± 5	0.019	0.012	0.088			
			^{3}He	116 ± 15	0.045	0.029	0.207			

[a] $\sigma_g = \pi R^2$ with $R = 1.5\,(A^{1/3} + a^{1/3})$, where A and a are target and projectile mass numbers.

[b] As the angular cone for p is approximately three times larger for t and ^{3}He, the total p yield is much larger than suggested by the comparison of the peak cross sections at 6°.

[c] The cross sections are for charged particles only. The breakup neutron yield is expected to be comparable to the proton yield.

would not produce an observable second lower energy peak.

We have attempted to test the assumption that the characteristics of the breakup peaks are dominated by the internal wave function and kinetic energy of the projectile. Using Eq. (1), we express the cross section in the c.m. frame of the projectile by transforming $\vec{p}_x$ to $\vec{p}$. The cross section $d\sigma/d\vec{p}$ is proportional to $|\phi(\vec{p})|^2$, the momentum distribution of the constituents in the projectile. This then allows a direct comparison of the momentum distribution $|\phi(\vec{p})|^2$ obtained in this manner with those derived from other experiments.

The internal momentum $\vec{p}$ is defined as positive for $p_x > P_\alpha \cos\theta_x$ and negative for $p_x < P_\alpha \cos\theta_x$ at a laboratory angle θ_x, where the minimum p is $p_\alpha \sin\theta_x$. Only at $\theta_x = 0°$ can $|\vec{p}| = 0$. As the angle increases the minimum momentum becomes larger, and the breakup yield decreases as a result of the decreasing probability for high momentum components. Figure 6 shows the data plotted in the c.m. frame of the alpha particle as a function of p for the deuteron channel at several angles for 20 and 40 MeV/nucleon alpha particles on ^{90}Zr. Similar plots are also given for several targets at $\theta_L = 6°$ in Fig. 7 in which the experimental data have been divided by $A^{1/3}$. Several interesting features emerge from such an analysis:

(1) The momentum distributions obtained from these data are generally in agreement with Eqs. (2) and (3).

(2) The data points, except the data on the "$-p$"

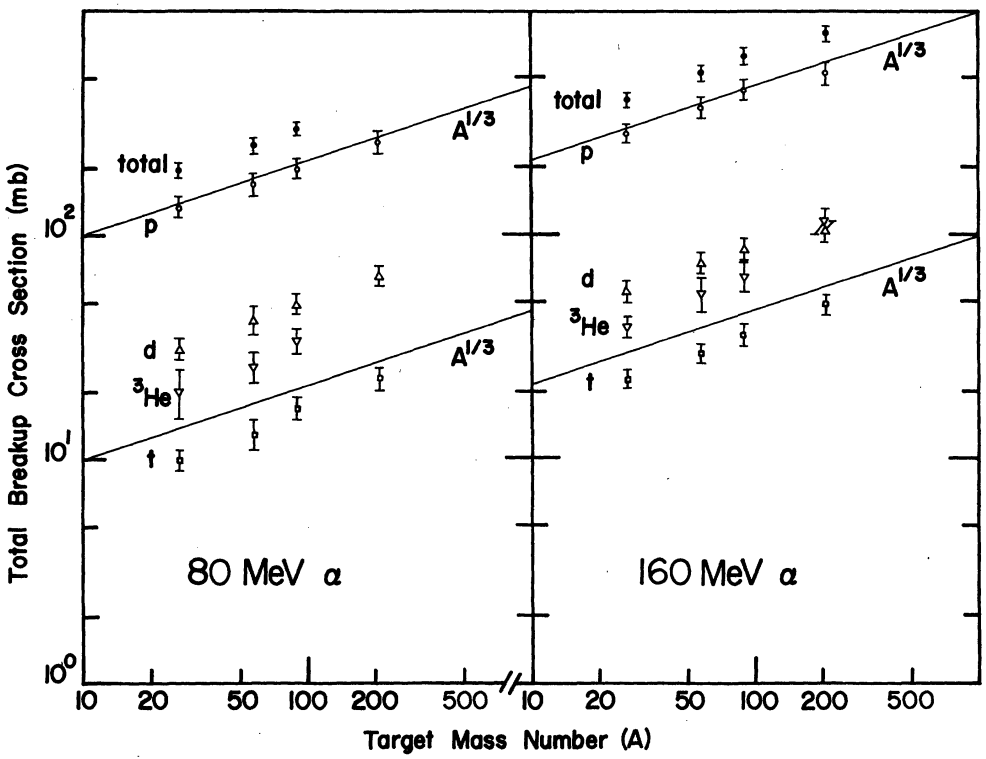

FIG. 5. The total breakup yield and breakup yield of each channel as a function of target mass for 80 MeV and 160 MeV alpha. It should be noted that the proton yield is distributed over a much larger region of phase space than the triton and ^{3}He yields, resulting in a significantly greater yield than indicated by comparisons of the peak cross sections at 6°.

side where other processes such as pre-equilibrium emissions are important, fall on the same distribution curves for different angles.

(3) The momentum distributions are approximately independent of the target nucleus.

(4) Distortion effects from the target nucleus do not seem to be important in terms of the spectral shapes.

These results are generally reminiscent of early studies of knockout reactions in which the spectral behaviors could be accounted for reasonably well by plane-wave calculations but the DWBA was required to fit the absolute magnitude.[15] The plane-wave breakup calculations clearly represent only a "first" order estimate. Nevertheless, the comparison of these calculations with data may provide a useful guide for the development of more realistic DWBA calculations.

V. CONCLUSION

The p, d, t, and ^{3}He energy spectra at forward angles resulting from the bombardment of target nuclei with 20 and 40 MeV/nucleon alpha particles show broad peaks at energies corresponding to the beam velocity. The locations, shapes, and widths of these peaks are roughly independent of the target nuclei from $A = 27$ to 209. The characteristics of the peaks are determined by the properties of the projectiles. These peaks are assumed to be due to the breakup of alpha particles in the nuclear field. The breakup cross section decreases rapidly with increasing angles and increases with increasing target mass and incident energy. The total breakup yield, summed over all charged fragments, accounts for 15–35% of the alpha-particle total reaction cross section and has an approximate $A^{1/3}$ dependence. The ratios of breakup yields among different fragments are roughly independent of the incident energy and the target nucleus. The $A^{1/3}$ dependence of breakup yield suggests that the breakup process is peripheral.

A simple plane-wave alpha-particle breakup model gives a rather good description of the experimental data. The characteristics of the breakup peaks are determined by the momentum distribution of the observed fragment in the projectile. The momentum distribution used is consistent with the results of quasifree scattering

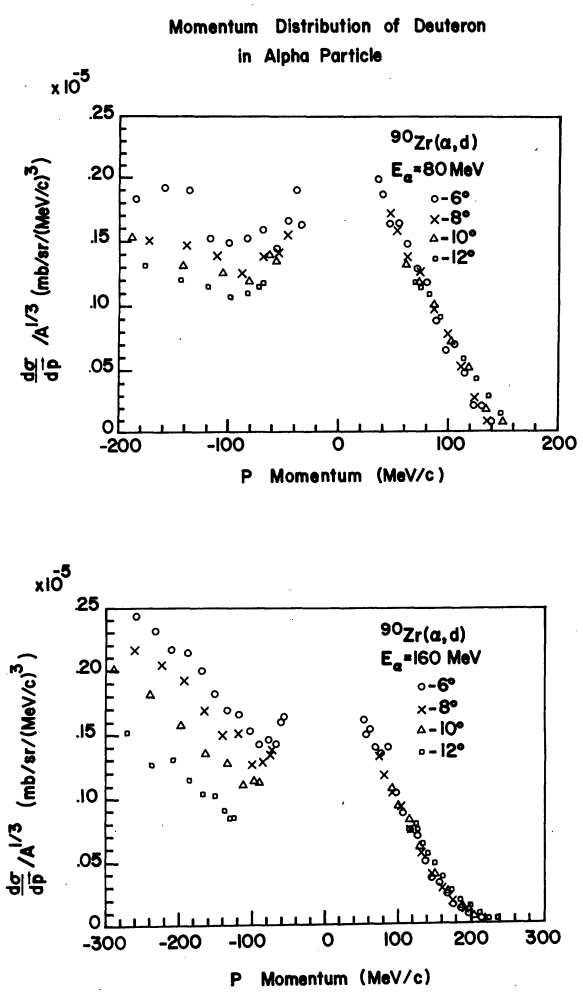

FIG. 6. The deuteron spectra plotted in the c.m. frame of alpha particles as a function of internal momentum p at several angles for 20 and 40 MeV/nucleon alpha particles on ^{90}Zr.

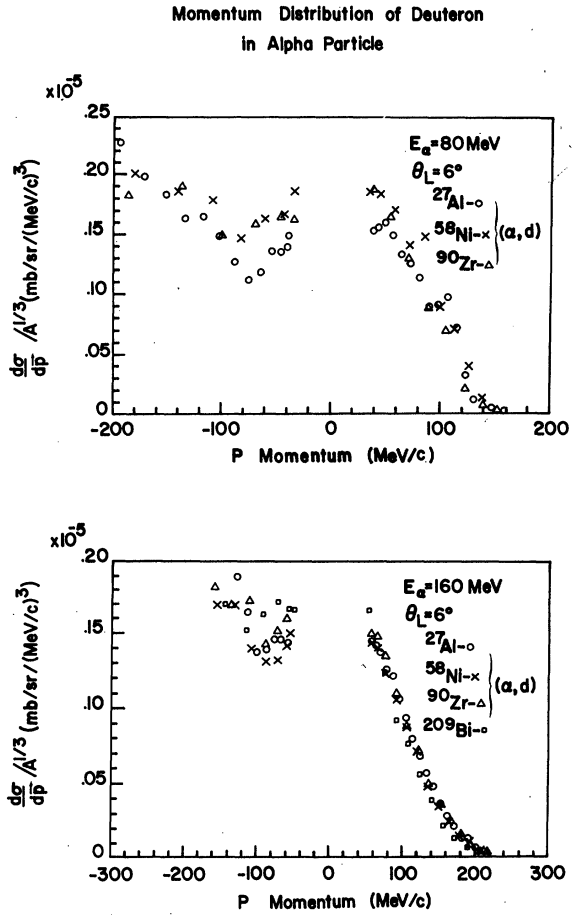

FIG. 7. Same as Fig. 6 for several targets at $\theta_L = 6°$, where experimental spectra have been divided by $A^{1/3}$.

and other reactions.[3,4]

A second peak at $\frac{1}{4}$ of incident energy is observed in the deuteron spectra. This peak may be due to a two-step breakup-pickup process involving an intermediate breakup nucleon. In order to understand the details of the projectile breakup, the particle-particle angular correlation measurements have been carried out and are being analyzed. The results of these measurements should shed light on the relative importance of the various mechanisms which contribute to the breakup of the projectile.

ACKNOWLEDGMENTS

A grant from the University of Maryland Computer Science Center for carrying out part of these analyses and calculations is acknowledged. This work was supported in part by the National Science Foundation.

*Present address: Oak Ridge National Laboratory, P.O. Box X, Oak Ridge, TN 37830.

[1]J. R. Wu, C. C. Chang, and H. D. Holmgren, Phys. Rev. Lett. 40, 1013 (1978).
[2]R. Serber, Phys. Rev. 72, 1008 (1947).
[3]T. K. Lim, Phys. Lett. 44B, 341 (1973).
[4]R. Frascaria *et al.*, Phys. Rev. C 12, 243 (1975).
[5]A. Budzanowski *et al.*, Phys. Rev. Lett. 41, 635 (1978).

[6]J. R. Wu, C. C. Chang, and H. D. Holmgren, Phys. Rev. C 19, 370 (1979); J. R. Wu, Ph.D. thesis, University of Maryland, 1977 (unpublished).
[7]G. Baur and D. Trautman, Phys. Rep. 25C, 293 (1976).
[8]N. Matsuoka *et al.*, Nucl. Phys. A311, 173 (1978).
[9]C. M. Castaneda, M. A. Smith, Jr., T. E. Ward, and T. R. Nees, Phys. Rev. C 16, 1437 (1977); C. M. Castaneda *et al.*, Phys. Lett. 77B, 371 (1978).
[10]C. K. Gelbke *et al.*, Phys. Lett. 71B, 83 (1977).
[11]R. W. Koontz, C. C. Chang, H. D. Holmgren, and J. R. Wu (unpublished).
[12]J. R. Wu, C. C. Chang, and H. D. Holmgren, Phys. Rev Rev. C 19, 659 (1979).
[13]C. C. Chang, H. D. Holmgren, R. W. Koontz, and J. R. Wu (unpublished).
[14]J. R. Wu, C. C. Chang, and H. D. Holmgren, Phys. Rev. C 19, 698 (1979).
[15]M. Jain, P. G. Roos, H. G. Pugh, and H. D. Holmgren, Nucl. Phys. A153, 49 (1970).